Available online at www.sciencedirect.com
ScienceDirect
International Journal of Heat and Mass Transfer 50 (2007) 196–207
International Journal of HEAT and MASS TRANSFER
www.elsevier.com/locate/ijhmt

Influence of sintering on the growth rate of particulate fouling layers

M.S. Abd-Elhady [a,*], S.H. Clevers [a], T.N.G. Adriaans [a], C.C.M. Rindt [a], J.G. Wijers [b], A.A. van Steenhoven [a]

[a] Department of Mechanical Engineering, Eindhoven University of Technology, P.O. Box 513, 5600 MB Eindhoven, The Netherlands
[b] Department of Chemical Engineering, Eindhoven University of Technology, P.O. Box 513, 5600 MB Eindhoven, The Netherlands

Received 11 August 2005; received in revised form 11 April 2006
Available online 22 August 2006

Abstract

This article addresses the question; why the gas-side temperature affects the rate of particulate fouling of heat exchangers? An experiment was carried out in a gas-cooler of a full-scale biomass gasifier to investigate the influence of the gas-side temperature on the strength, structure and growth rate of particulate fouling layers. It is observed that the particulate fouling rate in the gas cooler decreases with sintering, which is a function of the gas-side temperature. Detailed impaction experiments are carried out to investigate the influence of sintering on the removal of particles from a particulate fouling layer due to an incident particle impact as well as the sticking of an incident particle to a particulate fouling layer. Sintering of a fouling layer lowers significantly the ability of an incident particle to stick to the fouling layer or to remove particles out of the layer. However, particles that are still able to deposit on the sintered fouling layer will not sinter immediately, and can be removed due to the incident particles impact. The removal of newly deposited particles on a fouling layer due to incident particles becomes easier as sintering of the fouling layer takes place. Accordingly, it may be stated that sintering reduces the fouling rate of heat exchangers by lowering the deposition of new particles and increasing the removal rate of newly deposited particles. This explains why the growth rate of particulate fouling layers decreases with the gas-side temperature.
© 2006 Elsevier Ltd. All rights reserved.

Keywords: Particulate fouling; Sintering; Heat exchanger

1. Introduction

One of the challenges in the operation of biomass gasifiers is particulate fouling. Particulate fouling is defined as the accumulation of particles on a heat transfer surface that form an insulating layer, which reduces the rate of heat transfer and can lead to operation failure as has been reported by many researchers, e.g. in waste incinerators by van Beek et al. [1], in a coal-fired power plant by Bryers [2] and in utility scale boilers by Gupta et al. [3]. van Beek et al. [1] observed that the fouling layers on the economizer tubes of a Dutch waste incinerator, where the lowest gas-side temperature exists, were powdery, however on the superheater, where the highest gas-side temperature exists, they were sintered. The thermal resistance of the fouling layer on the economizer tubes was higher than that of the superheater. Grillot and Icart [4] introduced a mass accumulation probe [5] in a diesel exhaust gas stream and monitored the fouling behaviour of the probe. From their experiments it can be concluded that increasing the gas-side temperature while keeping the gas velocity constant, results in reducing the final fouling layer thermal resistance and decreasing the fouling rate. Many efforts have been made by numerous researchers to understand and control fouling in heat exchangers [6–10]. The question that we would like to address in this article is why the gas-side temperature affects the rate of particulate fouling of heat exchangers.

According to Senior [11], as the fouling layer thickness increases with time, its thermal resistance increases too,

* Corresponding author. Tel.: +31(0)40 2473172; fax: +31(0)40 2433445.
E-mail address: m.s.abdelhady@tue.nl (M.S. Abd-Elhady).

0017-9310/$ - see front matter © 2006 Elsevier Ltd. All rights reserved.
doi:10.1016/j.ijheatmasstransfer.2006.06.018

Nomenclature

A_o	overall surface area of a heat exchanger, m^2
CRV	critical removal velocity, m/s
D	diameter of a particle, m
k	thermal conductivity, W/m K
LMTD	logarithmic mean temperature difference, K
MST	minimum sintering temperature, °C
P	porosity
$\dot{Q}$	rate of heat transfer, W
$R_{o,i}$	initial overall thermal resistance, m^2 K/W
$R_{o,f}$	final overall thermal resistance, m^2 K/W
R_o	overall thermal resistance, m^2 K/W
R_f	fouling layer thermal resistance, m^2 K/W
SEM	scanning electron microscope
T	temperature, °C
t	time, s
X	diameter of the neck between two sintered particles, m

Greek symbols

α	local impact angle, rad
ΔT	temperature difference, °C
Δt	a period of time, s
δ	thickness, m

Subscripts

c	cold
f	final, fouling
h	hot
i	initial
o	overall

which results in an increase in the surface temperature of the fouling layer. If the surface temperature of the fouling layer becomes higher than a certain limit, which is known as the minimum sintering temperature [12], sintering takes place. The minimum sintering temperature is usually far below the melting point of the fouling layer material [13,14]. Sintering leads to the reduction of the void volume and reinforcement of the contact bridges between the particles of the fouling layer, Ristic [15], and is therefore responsible for strengthening of the fouling layer as has been measured by Skrifvars et al. [16,17]. The reduction in porosity during sintering also results in increased thermal conductivity as was observed by Rezaei et al. [18] for coal ashes and synthetic ash samples. The fouling rate is determined by the difference between the deposition and removal of particles on and from the fouling layer, Kern and Seaton [19]. Therefore, the effect of sintering on deposition and removal of particles should be studied, to answer the above question.

Removal of particles from sintered fouling layers during operation of heat exchangers can happen either due to a shear flow as has been studied by Cabrejos and Klinzing [20] and Al-Hayes and Winterton [21] or due to an incident particle impact as shown by Werner and Haff [22]. Müller-Steinhagen et al. [23] and Grillot and Icart [4] have shown that when the gas speed is increased particulate fouling is reduced. For powdery fouling layers, particulate fouling can be avoided when the gas speed is above the critical flow velocity, Abd-Elhady et al. [24]. However, due to sintering, the fouling layer hardens in time and can become strong enough such that removal of particles by shear flow becomes ineffective, as found by Frederick et al. [25,26], Barnhart and Williams [27] and Senior [11]. In this research, the sticking of an incident particle on a sintered layer as well as the removal of particles from a sintered fouling layer due to an incident particle impact are studied experimentally as function of the impact speed and the degree of sintering. This is discussed in Section 2.

In Section 3, the results of the impaction experiments are compared with an experiment carried out in a gas-cooler of a full-scale biomass gasifier. The experiment in the gas-cooler was done to investigate the influence of the gas-side temperature on the strength, structure and growth rate of the fouling layer. The different sections of the gas-cooler were knocked after 21 h of operation, to see how strong particulate fouling layers become during operation and whether they will remain on the tubes or fall off. Samples of fouling layers were taken from the gas-cooler to measure the porosity and to investigate the change in the fouling layer structure during fouling. The minimum sintering temperature of the fouling layer was measured and compared to the operating gas-side temperature. Based on the knocking experiments, the porosity measurements, the impaction experiments and the relation between the minimum sintering temperature and the gas-side temperature, the fouling process is described and the influence of the gas-side temperature on the fouling rate of heat exchangers is discussed in Section 4. Finally in Section 5, the conclusions are presented.

2. Detailed impaction experiments

2.1. Experimental setup and experimental procedure

An experimental set-up has been built to determine the vertical impact speed, at which an incident particle sticks, bounces off or removes particles from a bed of particles, i.e. the fouling layer. The set-up consists of a vertical vacuumed column in which particles are released from a particle feeder onto a horizontal bed of particles, as shown

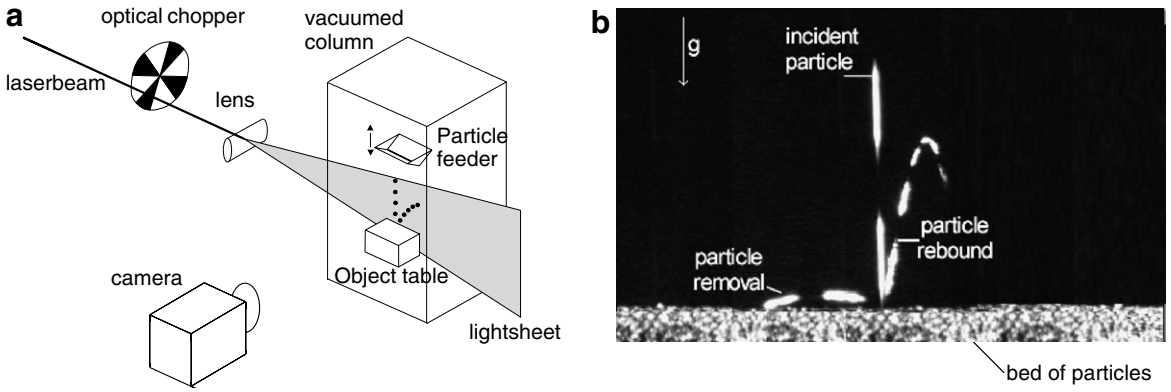

Fig. 1. The experimental set-up (a) and a typical recorded image (b) showing removal of particles from the fouling layer due to an incident particle impact. g is the direction of gravity.

in Fig. 1. The bed of particles is installed at the bottom of the vacuumed column on an object table. Varying the height of drop (height of the vacuum column) may lead to change the vertical impact speed of the incident particle, which is the speed of the particle in the direction of gravity. The vertical impact speed of the incident particle is varied from 0.01 to 3.5 m/s. The impact speed, impact angle and the number of particles that evolve due to an incident particle impact are measured. The impact of particles is recorded using a digital camera system. A pulsated light sheet illuminates the particle several times in one camera image. The impact velocity is determined from the average distance between two successive illuminations (blobs) and the rate of pulsation of the laser sheet for each particle. The angle 2θ, which is the angle between the incident and the rebound trajectories of the incoming particle is determined graphically from the recorded image. The angle 2θ is used to deduce the local impact angle α of the incident particle. The local impact angle α is depicted in Fig. 2, and is defined as the angle between the center line of the colliding particles and the horizontal at the beginning of impact. Fig. 2 shows an incident particle falling vertically

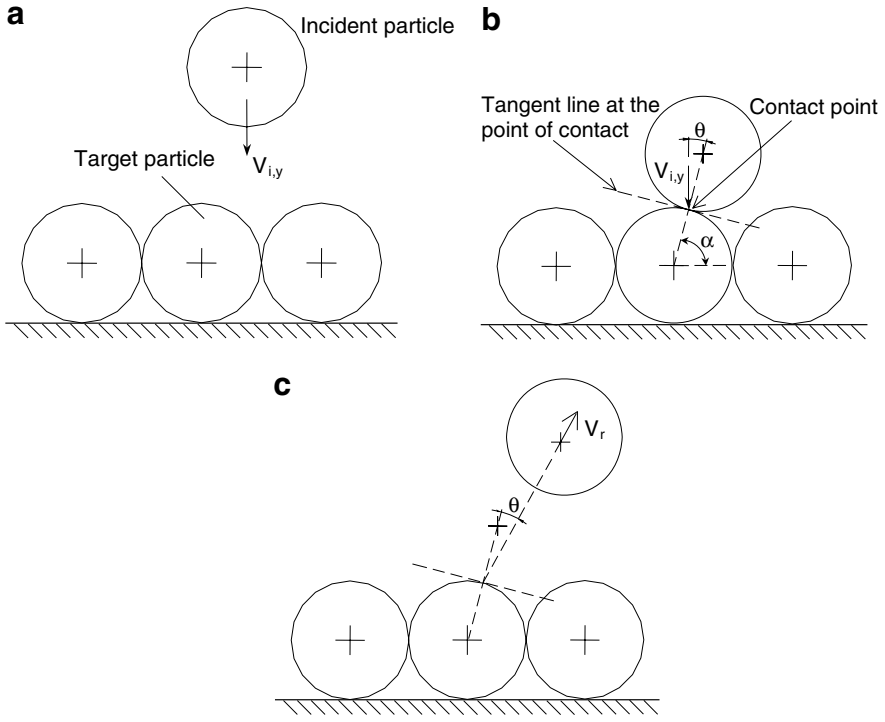

Fig. 2. An incident particle falling vertically (a) with a velocity $V_{i,y}$ onto a bed of particles, hitting the target particle (b) at an angle θ from the line of centers joining them and bouncing off (c) with a rebound velocity V_r. α is the angle between the line of centers of the colliding particles and the horizontal at the beginning of impact.

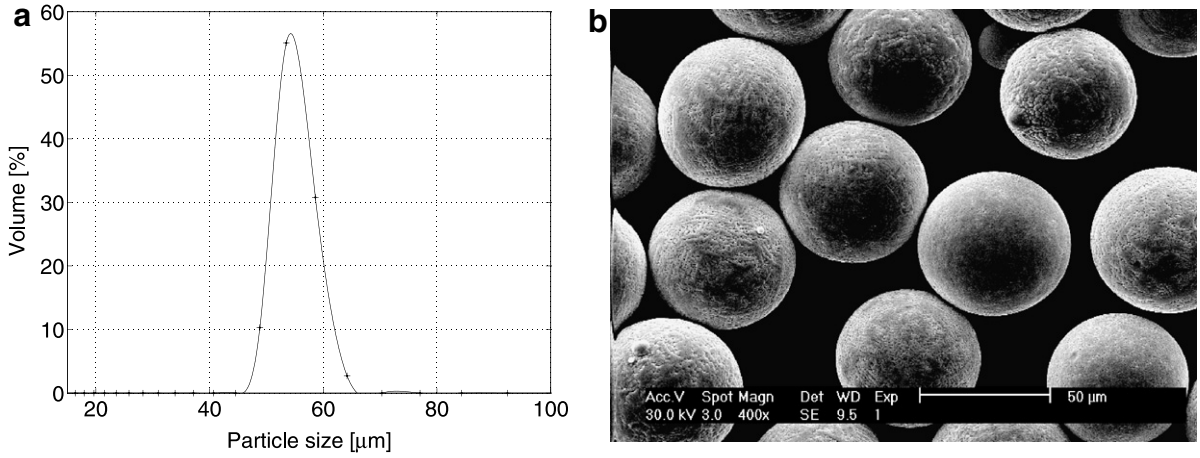

Fig. 3. Particle size distribution of the bronze particles used in the impaction experiments with an average diameter of 54 μm and a standard deviation of ±3 μm (a), and a scanning electron microscope image of the particles (b).

onto a bed of particles and then rebounding after impact. From Fig. 2, it can be concluded that the local impact angle α is equal to

$$\alpha = 90 - \theta. \quad (1)$$

Further details about the measurement procedure and analysis can be found in van Beek [28].

2.2. Sample preparation and particles used

The particles used in the impaction experiments and the fouling layers preparation are spherical bronze particles of average diameter 54 μm with a standard deviation of ±3 μm. The particle size distribution and a SEM image for the spherical bronze particles used, are shown in Fig. 3. Two fouling layers are prepared by placing the bronze particles in two sample holders of size 20 mm × 20 mm × 5 mm. One sample holder is placed in a tube oven with a nitrogen atmosphere for 20 h at 500 °C to prepare a sintered fouling layer, and the other sample holder represents a powdery fouling layer. Sintering of the bronze particles is done in a non-oxidizing nitrogen environment to avoid oxidation of the particles and changing their mechanical and material properties. A SEM image of the neck formed between two sintered particles in the 20-h sample is shown in Fig. 4. The degree of sintering is measured by the size of the neck formed, which is a function of the heating temperature and time [29,30]. The neck diameter of the powdery sample is 0 μm and of the 20 h-sample is 12 μm ± 1 μm. The neck diameter of the sintered layer was measured from the SEM images taken, where 20 particles were checked and the average diameter was calculated.

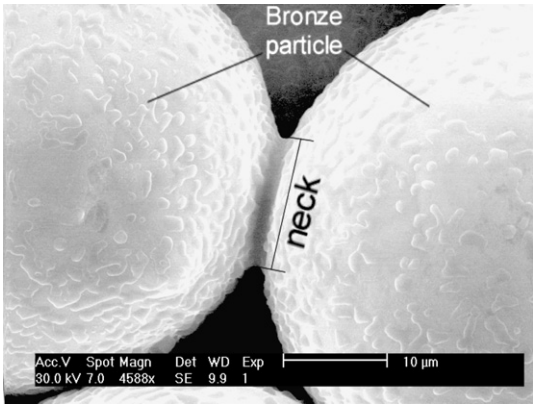

Fig. 4. Neck formed between two bronze particles sintered in nitrogen at 500 °C for 20 h.

2.3. Experimental results

The results of the impaction experiments for the powdery and the sintered fouling layers are shown in Fig. 5a and b, where the number of particles ejected is given as a function of the vertical impact speed of the incident particle. The number of particles ejected includes the incident particle, and a value of zero means that sticking occurs. The critical sticking velocity [31] is defined as the maximum impact speed at which an incident particle sticks to a bed of particles. From the experiments it is found that the critical sticking velocity is 0.3 m/s for a bronze particle with a diameter of 54 μm hitting a powdery layer and if the vertical speed of the incident particle is larger than 0.6 m/s particle removal can occur, as shown in Fig. 5a. The incident particle can rebound off the bed of particles if the vertical impact speed is between 0.18 m/s and 1.1 m/s. The overlapping in the number of particles ejected is due to the variation in the local impact angle α [32], i.e. the position where the incident particle hits the target particle, for the same vertical impact speed.

The critical sticking velocity for the sintered bronze layer was found to be 0.04 m/s, which is 7.5 times lower than the sticking velocity for the powdery layer, 0.3 m/s. Sintering strengthens the bonding between the bed particles and therefore the particles in the sintered layer can only

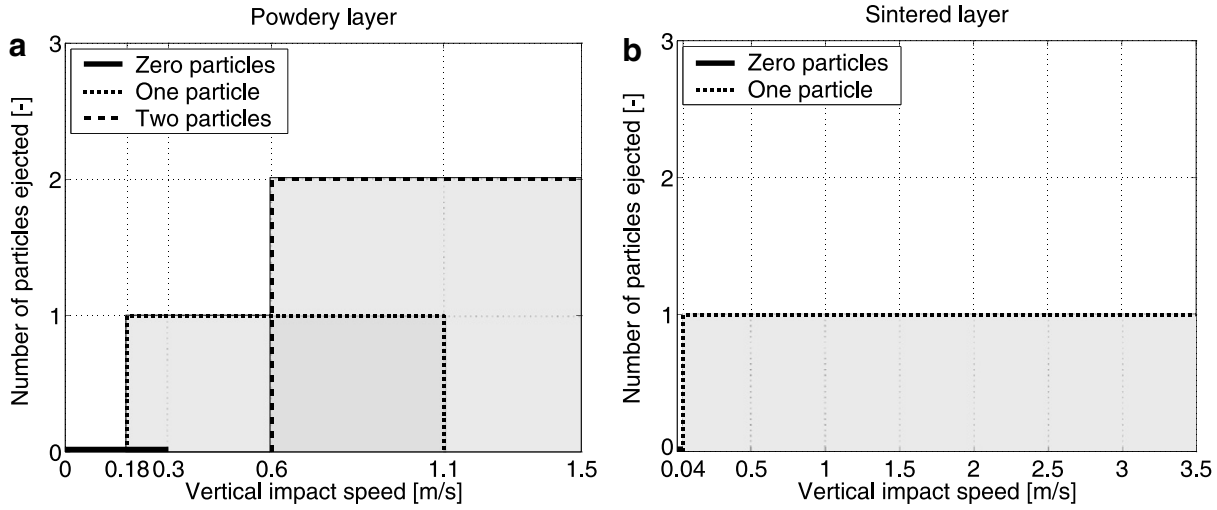

Fig. 5. Number of particles ejected from a powdery layer (a) and a sintered layer (b) due to an incident particle impact. The incident particle and the particles of the layer are of the same material, bronze, and average diameter, 54 μm.

move as a whole, which consequently reduces the kinetic energy lost by the incident particle to the bed of particles, and therefore lowers the critical sticking velocity. The removal of a bed particle, due to an incident particle impact, hardly occurs due to the strong bonding between the sintered bed particles. An incident particle with a vertical impact speed of 3.5 m/s still had not sufficient energy to remove a particle out of the layer, as has been seen from the experiments.

A second experiment was carried out to investigate the removal of particles from a fine-powdery layer of particles on top of the sintered layer due to an incident particle impact. This experiment was done to investigate the influence of sintering on the further growth of sintered fouling layers. The incident particle, the fine-powdery layer of particles and the sintered layer are all of the same particle size and material. The fine layer of particles was prepared by pouring a certain mass of particles in the cavity of the sample holder of the sintered layer such that one layer of particles covers the sintered layer. From the impaction experiment it was found that it was possible to remove particles out of the powdery layer at a vertical impact speed of 0.1 m/s and higher. This result is further used in Section 4 to explain the reduction in particulate fouling due to sintering.

3. Experimental results from the gas-cooler

3.1. Temperature measurements in the gas-cooler

An experiment was carried out in a gas-cooler of a full-scale biomass gasifier to investigate the influence of the gas-side temperature on the strength, structure and growth rate of the fouling layer. The hot gases coming from the biomass gasifier are cooled down from 950 °C to 450 °C by the mentioned gas-cooler, which consists of four consecutive sections, two evaporators (I and II) separated by a superheater and followed by an economizer, as shown in Fig. 6. The gas-cooler tubes were knocked after 21 h of operation. The performance of the different sections of the gas-cooler during operation is monitored through the respective inlet and exit gas/water temperatures. The inlet and exit gas/water temperatures are measured using thermocouples with an accuracy of ±0.5 °C. The water mass flow rate and pressure are measured with an accuracy of ±1% and ±0.4%, respectively. Based on an energy balance between the gas-side and the waterside in the gas-cooler, the mass flow rate of the hot gases passing through the gas-cooler is calculated.

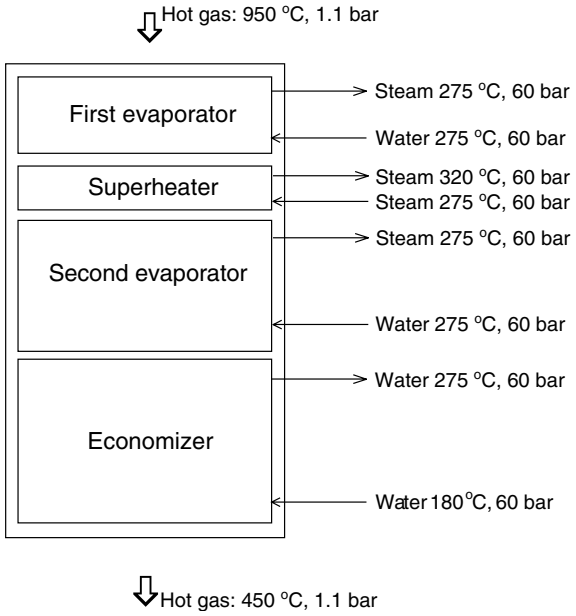

Fig. 6. Different sections of the gas-cooler, and the corresponding gas/water/steam temperatures and pressures.

The performance of the different sections of the gas-cooler before and after knocking is shown in Figs. 7 and 8.

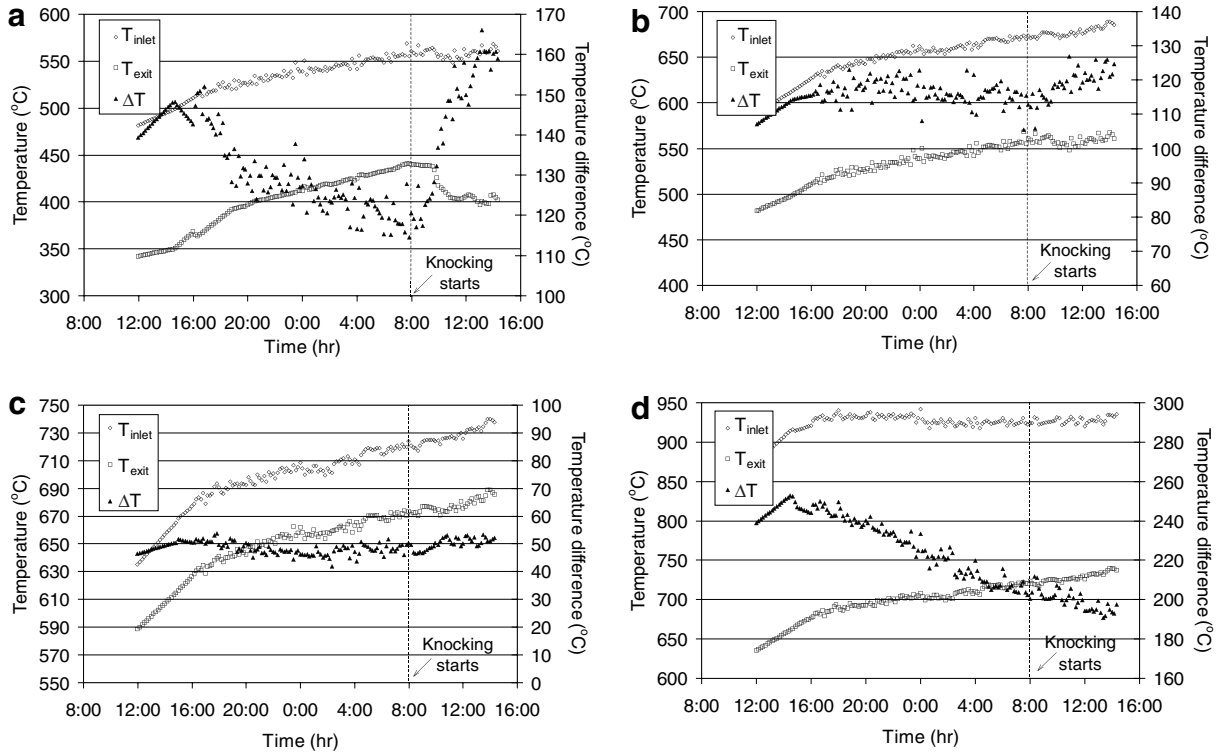

Fig. 7. Inlet and exit gas-side temperatures through the economizer (a), second evaporator (b), superheater (c) and first evaporator (d). ΔT is the temperature difference between inlet and outlet gas-side temperatures.

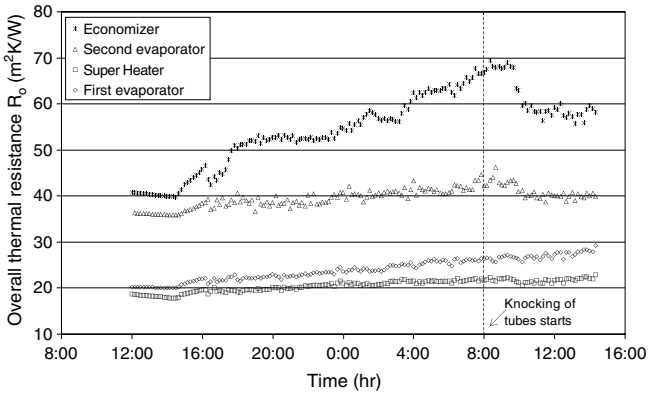

Fig. 8. The overall thermal resistance, R_o, of the different section of the gas-cooler during 24 h of operation.

Fig. 7 shows the inlet and exit gas temperatures of the economizer (Fig. 7a), second evaporator (Fig. 7b), superheater (Fig. 7c) and first evaporator (Fig. 7d). The gas-side temperature is highest at the first evaporator and lowest in the economizer section. The temperature difference, ΔT, between the inlet and outlet gas temperatures for each section of the gas-cooler is also plotted in Fig. 7. Fig. 8 shows the overall thermal resistance, R_o, across the different sections of the gas-cooler and is calculated from

$$R_o = \frac{A_o \times \mathrm{LMTD}}{\dot{Q}}, \tag{2}$$

where $\dot{Q}$ is the rate of heat transfer to the gas-cooler section considered and is calculated from the measured water/steam mass flow rate and the inlet and exit conditions of the water/steam. A_o is the overall tube bundle surface area of the gas-cooler section considered and LMTD is the logarithmic mean temperature difference. LMTD is calculated using the inlet and outlet temperatures on the water/steam side, i.e. the cold side, and the flue gas temperatures measured in front and behind the relevant gas-cooler section, i.e. the hot side, and is defined as [33]

$$\mathrm{LMTD} = \frac{\Delta T_1 - \Delta T_2}{\ln(\Delta T_1/\Delta T_2)}. \tag{3}$$

ΔT_1 and ΔT_2 are equal to

$$\begin{aligned} \Delta T_1 &= T_{\mathrm{h,inlet}} - T_{\mathrm{c,exit}}, \\ \Delta T_2 &= T_{\mathrm{h,exit}} - T_{\mathrm{c,inlet}}, \end{aligned} \tag{4}$$

where $T_{\mathrm{h,inlet}}$ and $T_{\mathrm{h,exit}}$ are the inlet and outlet temperatures at the gas-side, while $T_{\mathrm{c,inlet}}$ and $T_{\mathrm{c,exit}}$ are the inlet and outlet temperatures on the waterside. The subscripts h and c stand for the hot and the cold side, respectively.

The thermal resistances shown in Fig. 8 show a declining smooth pattern from the beginning of operation until about 15:00 h, and then a scattered pattern with an increasing thermal resistance. The smooth initial phase occurs in the warming-up period in which an external gas burner using natural gas is used to heat up the biomass in the gasifier until gasification can take place. In the warming-up period, the flue gases produced are almost free of particles, and the rate of heat transfer is enhanced due to the increase in turbulences around the heat exchanger tubes because of

the increase in the surface roughness of the tubes due to particulate fouling, Müller-Steinhagen [34] and Zettler et al. [35]. The heat transfer enhancement due to particulate fouling in the warming-up period over-rides the thermal resistance of the fouling layer causing a decrease in the overall thermal resistance. Once gasification has started, fly ashes and biomass particles are produced and entrained in the flue gases causing sever fouling of the gas-cooler tubes, which is responsible for the scatter in the temperature measurements and the increase in the overall thermal resistance as shown in Figs. 7 and 8, respectively.

The temperature difference between the inlet and exit gas-side temperatures at the economizer decreased until knocking of the tubes has started and increased after knocking as can be seen from Fig. 7a. Fig. 8 shows that the overall thermal resistance of the economizer increased with time before knocking and decreased after knocking, which indicates that the fouling layers were weakly attached to the economizer tubes, such that it was removed by tube knocking. The thermal resistances of the second evaporator and the superheater were less influenced by tube knocking compared to the economizer, as can be seen from Fig. 8. However, the first evaporator showed a different performance from the other gas-cooler sections as can be seen from Figs. 7 and 8. The temperature difference between the inlet and exit gas-side temperatures at the first evaporator decreased and the overall thermal resistance increased with time even after knocking, which indicates that the deposited fouling layers were strongly attached to the first evaporator tubes and tube knocking is not effective in removing them.

3.2. Porosity measurements of the fouling layers

Samples were taken from the fouling layers on the superheater and the first evaporator tubes to measure its porosity. It was not possible to take samples from the fouling layers in the economizer due to its powdery and fragile structure and from the second evaporator because it was out of reach. The porosity of the fouling layer was measured using quantitative microscopy [36] as a function of the fouling layer thickness. The porosity was determined by embedding the fouling layer in epoxy, cross sectioning the fouling layer and polishing the sample for imaging using a scanning electron microscope (SEM). Images created by the SEM had a dark background of epoxy and a light grey colour of the embedded fouling layer particles, and they were transformed into black and white pictures, where the fouling layer particles are white and the epoxy, i.e. air pockets, is black. The surface porosity was determined by the percentage of black pixels in the image, which can be taken as volume porosity. According to Delesse's principle [37], the surface porosity represents the volume porosity if the porosity is randomly distributed. The porosity was measured near the top, middle and bottom of the fouling layer and the results for the fouling layer taken from the superheater are shown in Fig. 9 and Table 1. It can be concluded from the porosity measurements that the porosity of the fouling layer decreases from the top, i.e. near the hot gas-side, to the bottom, i.e. near the cold waterside. SEM images of the bottom and top of the fouling layer taken from the superheater are shown in Fig. 10. These images show that the fouling layer structure is

Table 1
Porosity measurements at different positions in the fouling layer taken from the superheater

Location of porosity measurement	Porosity
Bottom of the fouling layer, i.e. near the heat exchanger tube	60%
Middle cross section	25–40%
Top of the fouling layer, i.e. near the gas-side	15%

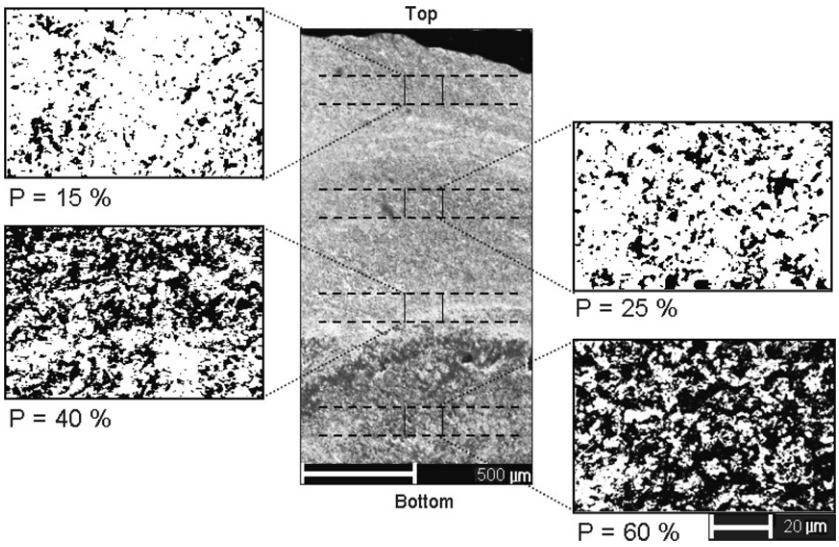

Fig. 9. Porosity measurements at different positions in the fouling layer taken from the superheater. White represents material and black represents void space (epoxy). The top of the fouling layer was near the hot gas-side while the bottom of the layer was near the relatively cold heat exchanger tube.

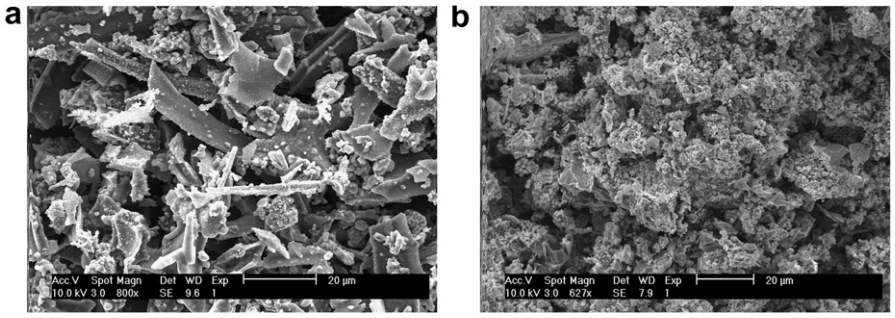

Fig. 10. SEM images of the bottom of the fouling layer (a), i.e. near the relatively cold heat exchanger tube and top of the fouling layer (b), i.e. near the hot gas-side. The fouling layer was taken from the superheater.

Table 2
Element analysis for the fouling layers found on the tubes of the first evaporator and the superheater

Elements found in the fouling layers	C	O	Na	Si	Al	Mg	S	Cl	Ca	Ti	Pb	Zn

powdery and porous at the bottom, while at the top the structure is condensed and robust. A similar change in the microstructure of sintered ash deposits found on the convective pass of a utility scale boiler is reported by Robinson et al. [38]. The fouling layer taken from the first evaporator has a porosity variation similar to the superheater except that the top of the sample has a solidified microstructure, i.e. the porosity is equal to zero, which indicates that local melting has occurred at the top surface of the fouling layer during operation of the gas-cooler.

3.3. Measurement of the fouling layer minimum sintering temperature

Samples were taken from the fouling layer on the superheater to measure its minimum sintering temperature [39,40]. The samples are crushed into fine particles of a size smaller than 56 μm, to ensure that the particle size resembles the original state of the fouling layer before sintering, i.e. the fly ashes. Elements of the fouling layer were determined using the energy dispersive X-ray analysis and the results are shown in Table 2. The element analysis showed the existence of volatile elements such as lead and zinc and the existence of oxidizable elements such as carbon. The element analysis showed a big percentage of carbon in the fouling layer, i.e. above 50% by weight. The crushed layer was placed in an airtight aluminum oxide container to ensure that oxidation and evaporation of volatile elements were prevented. The samples were placed in an oven for 20 h at different temperatures, and then examined under the scanning electron microscope. It was found that at an oven temperature of 675 °C the sample was still powdery, Fig. 11a. The sample showed sintering at a temperature of 750 °C, Fig. 11b. and a larger degree of sintering at 800 °C, Fig. 11c. Due to sintering, the sample structure has changed from a powdered nature to a solidified nature. It can be concluded that the minimum sintering temperature of the fouling layer is between 675 °C and 750 °C.

4. Fouling process description and discussion

The average rate of change in the overall thermal resistance R_o before knocking is calculated as follows:

$$\frac{dR_o}{dt} = \frac{R_{o,i} - R_{o,f}}{\Delta t}, \tag{5}$$

where $R_{o,i}$ and $R_{o,f}$ are the overall thermal resistance at the beginning of operation and just before knocking, respectively. Δt is the time period between the beginning of operation and the point of knocking. It is assumed that the average rate of change in the fouling layer thermal resistance R_f is equal to the average rate of change in the overall thermal resistance R_o, i.e.

$$\frac{dR_f}{dt} = \frac{dR_o}{dt}. \tag{6}$$

The fouling layer thermal resistance R_f, expressed in [m^2 K/W], is related to its thermal conductivity k and thickness δ by

$$R_f = \frac{\delta}{k}. \tag{7}$$

The increase in the fouling layer thermal resistance during fouling is an indication of the fouling layer growth if the thermal conductivity of the fouling layer increases or remains constant, which are the cases when sintering or no sintering takes place [38], respectively. The average rate of change in the thermal resistance of the fouling layer is taken as a measure for the growth of the fouling layer, i.e. the fouling rate. The average rate of change in the fouling layer thermal resistance before knocking, dR_f/dt, is plotted in Fig. 12 as a function of the average gas-side temperature across the different sections of the gas-cooler except for the first evaporator. The first evaporator is not included in Fig. 12, because slagging [41] has occurred, i.e. local melting at the fouling layer surface due to the high gas-side temperature, which is different from particulate

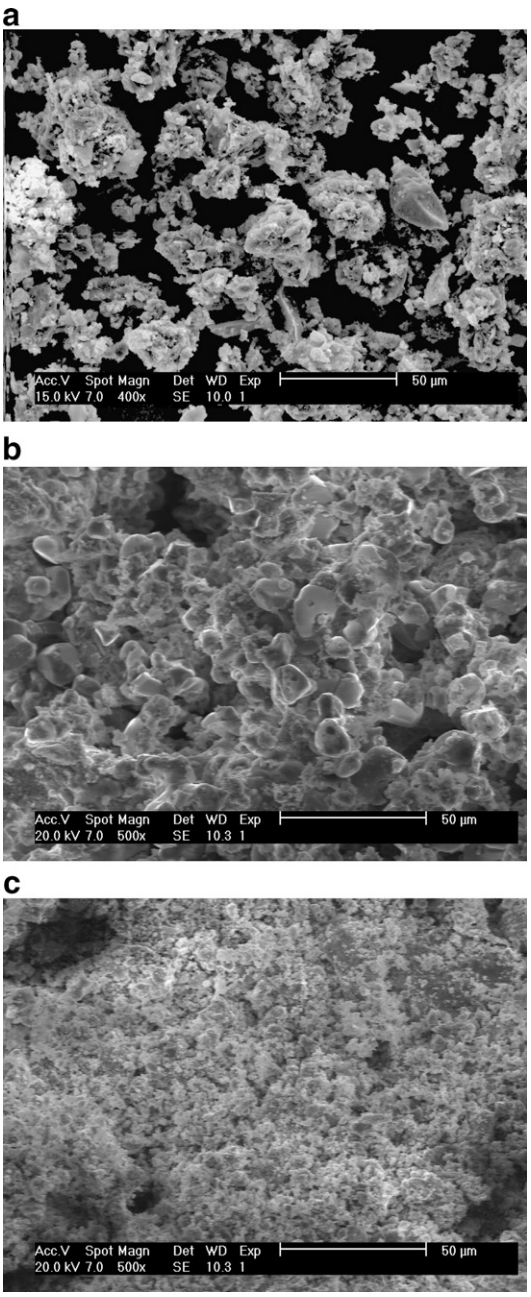

Fig. 11. SEM images of the fouling layer particles, which were heated for 20 h at different temperatures, showing no sintering at 675 °C (a), sintering at 750 °C (b) and a high grade of sintering at 800 °C (c).

fouling. The average rate of change in the fouling layer thermal resistance in case of the economizer is larger than that of the second evaporator and the superheater, i.e.

$$\left.\frac{dR_f}{dt}\right|_{\text{economizer}} > \left.\frac{dR_f}{dt}\right|_{\text{second evaporator}} > \left.\frac{dR_f}{dt}\right|_{\text{super heater}}. \quad (8)$$

The decrease in the average rate of change in the fouling layer thermal resistance, i.e. the fouling rate, for the higher gas-side temperatures is in agreement with the work of Grillot and Icart [4]. The average gas velocity in the different sections of the gas-cooler is calculated from the mass

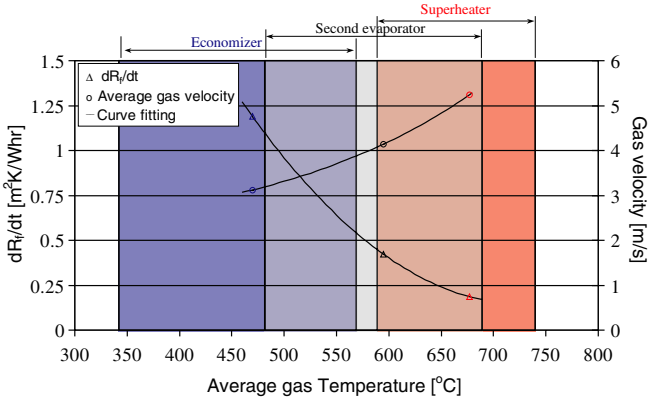

Fig. 12. The average rate of change in the fouling layer thermal resistance, dR_f/dt, and the average gas velocity before knocking versus the average gas-side temperature across the different sections of gas-cooler. The shaded areas represent the range of the gas-side temperature in the corresponding gas-cooler section.

flow rate, the corresponding gas density and the corresponding gas-cooler free cross sectional area. The average gas velocity versus the average gas-side temperature across the different sections of the gas-cooler is plotted in Fig. 12, except for the first evaporator for the same reason as mentioned before. The average gas speed is lowest in the economizer, 3.1 m/s, and highest in the superheater, 5.2 m/s, which shows that there is not a big variation between the gas velocities in the economizer and the superheater. The ratio between the gas velocities in the economizer and the second evaporator is 0.6, and the ratio between the gas velocities in the economizer and the superheater is 0.75. The ratio between the fouling rates in the economizer and the second evaporator is 2.8, and the ratio between the fouling rates in the economizer and the superheater is 6.4, which makes it plausible to assume that the small increase in the gas velocity across the gas-cooler cannot alone explain the large decrease in the fouling rate as shown in Fig. 12. The fouling process in the economizer and the superheater is further discussed in the next sections to explain the decrease in the fouling rate as the gas-side temperature increases in terms of the critical sticking and removal velocities and the microstructure change in the fouling layer.

4.1. Particulate fouling in the economizer and the superheater

The knocking experiment shows that the fouling layers deposited on the economizer tubes, where the lowest gas temperature exists, have been strongly affected by knocking such that a big portion of the fouling layer has fallen off from the tubes, as can be seen from Figs. 7a and 8. The range of the gas-side temperature in the economizer is 340–570 °C, which is lower than the measured minimum sintering temperature of the deposits, 675–750 °C. This implies that the fouling layer on the economizer stays powdery, which makes it relatively easy to remove by knocking.

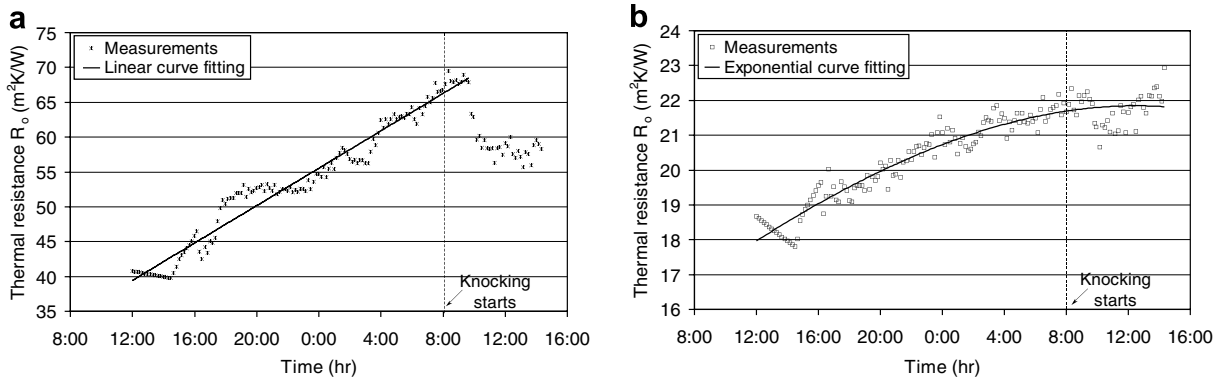

Fig. 13. Curve fitting of the overall thermal resistance R_o of the economizer (a) and the superheater (b).

The measured thermal resistance of the economizer is presented in Fig. 13a, which shows a continuous increase in thermal resistance due to fouling till knocking, and then a drop in the thermal resistance after knocking. The continuous increase in the thermal resistance can be explained by the observation that the critical sticking and removal velocities for powdery layers become constant and independent of the layer thickness, if the thickness is larger than a certain limit, as was found from the numerical simulations done by Abd-Elhady [32]. The stabilization of the critical removal and sticking velocities as the fouling layer thickens in time, indicates a constant fouling rate and a linear increase in the fouling layer thermal resistance, which is in agreement with the measurements shown in Fig. 13a.

The range of the gas-side temperatures in the superheater is mostly in range with the minimum sintering temperature (MST) of the deposits, which implies that the surface of the particulate fouling layers on the superheater can be sintered. Porosity measurements presented in Section 3.2 have shown that there is a porosity reduction with the fouling layer thickness, which indicates that sintering of the fouling layer has taken place during operation. The knocking experiment has shown that the thermal resistance of the superheater tubes has hardly been affected by tube knocking as can be seen from Fig. 8, which is another indication that sintering has taken place. The measured thermal resistance of the superheater is shown in Fig. 13b, which shows that there is an asymptotic behaviour of the thermal resistance. By comparing Fig. 13a to Fig. 13b, i.e. the no sintering case to the sintering case, it can be concluded that sintering is the main cause for the reduction in the fouling rate.

From the impaction experiments, it can be concluded that the critical sticking velocity decreases with the degree of sintering X/D, where X is the diameter of the neck formed between the sintered particles and D is the diameter of the particles, as can be seen from Fig. 5 and Table 3. The critical removal velocity which is defined as the minimum impact speed at which an incident particle can remove a particle out of a bed of particles increases with the degree of sintering due to the strong adhesion between the sintered particles as was found from the impaction experiments,

Table 3
The critical velocities for a powdery and a sintered bronze layers

	Fouling layer		
	Powdery	Sintered layer	Ratio $= \frac{\text{Powdery}}{\text{Sintered}}$
Degree of sintering, X/D^*	0	0.22	0
Critical sticking velocity	0.3 m/s	0.04 m/s	7.5
Critical removal velocity for the fouling layer	0.6 m/s	>3.5 m/s	Unknown
Critical removal velocity for a single-powdery layer on the fouling layer	0.6 m/s	0.1 m/s	6

The bronze particles are of average diameter of 54 μm.
* X is the diameter of the neck between the sintered particles and D is the diameter of the particles.

Fig. 5. However, in order to model the growth rate of sintered fouling layers we should look to both, the removal of particles from the sintered layer itself and the removal of the newly deposited particle on the sintered layer. The removal of particles deposited on the sintered layer due to incident particles of the same diameter and material was experimentally investigated, and it was found that the critical removal velocity (CRV) for a single-powdery layer of particles on the sintered layer is 0.1 m/s, which is lower than the CRV for a powdery layer by six times, as shown in Table 3. This indicates that sintering of a fouling layer reduces the CRV of the newly deposited layers, which consequently increases the removal rate of the newly deposited particles. The change in the fouling layer microstructure from powdery to sintered decreases the deposition rate of particles and increases the removal rate of newly deposited particles, which results in a reduction in the fouling rate as shown in Fig. 12 and as given by inequality (8).

5. Conclusions

An experiment was carried out in a gas-cooler of a full-scale biomass gasifier to investigate the influence of the gas-side temperature on the strength, structure and growth rate of particulate fouling layers. It is observed that the fouling layer on the economizer tubes where the

gas-side temperature is lower than the minimum sintering temperature (MST) of the layer has a powdery structure, while the fouling layer on the superheater tubes where the gas-side temperature is higher than the layer MST has a sintered robust structure. It is also observed that the fouling rate in the economizer is much higher than the fouling rate in the superheater. Deposited particles on the surface of heat exchangers form initially a powdery fouling layer stuck to the heat exchanger surface. As the fouling layer builds up, the thermal resistance of such layer increases and therefore its outer surface temperature increases too. When such outer surface temperature exceeds the MST of the ash deposits, sintering of the outer surface occurs which is the case in the superheater. Sintering stimulates the neck growth between ash deposits, which transforms the powdery fouling layer into a robust sintered layer.

Detailed impaction experiments have been performed to assign the critical sticking and removal velocities of a particle hitting a fouling layer as a function of the fouling layer degree of sintering. From the impaction experiments it is found that the critical sticking velocity of an incident particle hitting a powdery layer is much larger than the sticking velocity of a particle hitting a sintered layer. The formation of powdery layers at the beginning of a particulate fouling process increases the critical sticking velocity of the incident particles; hence, it enhances the fouling rate. Sintering of a fouling layer lowers significantly the ability of an incident particle to stick or to remove any particle out of the layer. However, particles that are still able to deposit on a sintered fouling layer will not sinter immediately, and can be removed due to the incident particles impact. The critical removal velocity of a particle hitting a powdery layer is larger than the removal velocity of a particle hitting a fine-powdery layer on top of a sintered layer. Therefore, the removal of newly deposited particles on a fouling layer due to incident particles becomes easier as sintering takes place. Accordingly, sintering reduces the fouling rate in heat exchangers by lowering the deposition rate of new particles and by increasing the removal rate of newly deposited particles. The growth rate of particulate fouling layers decreases with the gas-side temperature if sintering of the fouling layer takes place.

References

[1] M.C. van Beek, C.C.M. Rindt, J.G. Wijers, A.A. van Steenhoven, Analysis of fouling in refuse waste incinerators, Heat Transfer Eng. 22 (1) (2001) 22–31.

[2] R.W. Bryers, Fireside slagging, fouling and high temperature corrosion of heat-transfer surface due to impurities in steam-raising fuels, Prog. Energy Combust. Sci. 22 (1996) 29–120.

[3] R.P. Gupta, T.F. Wall, L.L. Baxter, The thermal conductivity of coal ash deposits: relationships for particulate and slag structures, in: R.P. Gupta, T.F. Wall, L.L. Baxter (Eds.), The Impact of Mineral Impurities in Solid Fuel Combustion, Kluwer Academic Press, New York, 1999, pp. 65–84.

[4] J.M. Grillot, G. Icart, Fouling of a cylindrical probe and a finned tube bundle in a diesel exhaust environment, Exp. Therm. Fluid Sci. 14 (1997) 442–454.

[5] J.D. Isdale, Debate on gas side fouling, in: L.F. Melo, T.R. Bott, C.A. Bernardo (Eds.), Fouling Sci. Technol., Kluwer publisher, Boston, MA, 1988, pp. 731–733.

[6] J. Taborek, T. Aoki, R.B. Ritter, J.W. Palen, I.G. Kundsen, Predictive methods for fouling behaviour, Chem. Eng. Prog. 68 (1972) 69–78.

[7] M. Bohnet, Fouling of heat-transfer surfaces, Chem. Eng. Technol. 10 (1987) 113–125.

[8] T.R. Bott, The Fouling of Heat Exchangers, Elsevier Science, New York, 1995.

[9] N. Epstein, Thinking about heat transfer fouling: a 5×5 matrix, Heat Transfer Eng. 4 (1) (1983) 43–56.

[10] J. Taborek, T. Aoki, R. Ritter, J.W. Palen, Fouling: the major unresolved problem in heat transfer, Chem. Eng. Prog. 68 (1972) 59–67.

[11] C.L. Senior, Predicting removal of coal ash deposits in convective heat exchangers, Energy Fuels 11 (1987) 416–420.

[12] A.Y. Al-Otoom, G.W. Bryant, L.K. Elliott, B.J. Skrifvars, M. Hupa, T.F. Wall, Experimental options for determining the temperature for the onset of sintering of coal ash, Energy Fuels 14 (2000) 227–233.

[13] B.J. Skrifvars, M. Hupa, Sintering of ash during fluidized bed combustion, Ind. Eng. Chem. Res. 31 (1992) 1026–1030.

[14] G.C. Kuczynski, Self-diffusion in sintering of metallic particles, Trans. Am. Inst. Min. Metal 185 (1949) 169–178.

[15] M.M. Ristic, Sintering – New Developments, Elsevier Scientific Publisher Company, Amsterdam, 1979.

[16] B.J. Skrifvars, M. Hupa, R. Backman, M. Hiltunen, Sintering mechanisms of FBC ashes, Fuel 73 (2) (1994) 171–176.

[17] B.J. Skrifvars, R. Backman, M. Hupa, Characterization of the sintering tendency of ten biomass ashes in FBC conditions by a laboratory test and by phase equilibrium calculations, Fuel Process. Technol. 56 (1998) 55–67.

[18] H.R. Rezaei, R.P. Gupta, G.W. Bryant, J.T. Hart, G.S. Liu, C.W. Bailey, T.F. Wall, S. Miyamae, K. Makino, Y. Endo, Thermal conductivity of coal ash and slags and models used, Fuel 79 (2000) 1697–1710.

[19] D.Q. Kern, R.E. Seaton, A theoretical analysis of thermal surface fouling, Chem. Eng. Prog. 4 (1959) 258–262.

[20] F.J. Cabrejos, G.F. Klinzing, Incipient motion of solid particles in horizontal pneumatic conveying, Powder Technol. 72 (1992) 51–61.

[21] R.A.M. Al-Hayes, R.H.S. Winterton, Bubble diameter on detachment in flowing liquids, Int. J. Heat Mass Transfer 24 (1981) 223–230.

[22] B.T. Werner, P.K. Haff, The impact process in Aeolian saltation: two-dimensional simulations, Sedimentology 35 (1988) 189–196.

[23] H. Müller-Steinhagen, F. Reif, N. Epstein, P. Watkinson, Influence of operating conditions on particulate fouling, Can. J. Chem. Eng. 66 (1988) 42–50.

[24] M.S. Abd-Elhady, C.C.M. Rindt, J.G. Wijers, A.A. van Steenhoven, E.A. Bramer, T.H. van der Meer, Minimum gas speed in heat exchangers to avoid particulate fouling, Int. J. Heat Mass Transfer 47 (17-18) (2004) 3943–3955.

[25] W.J. Frederick, E.K. Vakkilainen, Sintering and structure development in alkali metal salt deposits formed in Kraft recovery boilers, Energy Fuels 17 (2003) 1501–1509.

[26] W.J. Frederick, E.K. Vakkilainen, H.N. Tran, S.J. Lien, The conditions for boiler bank plugging by sub micrometer sodium salt (fume) particles in Kraft recovery boilers, Energy Fuels 18 (3) (2004) 795–803.

[27] D.H. Barnhart, P.C. Williams, The sintering test, an index to ash-fouling tendency, Trans. ASME 78 (1956) 1229–1236.

[28] M.C. van Beek, Gas-side fouling in heat-recovery boilers, Ph.D. Thesis, Eindhoven University of Technology, The Netherlands, 2001.

[29] J. Frenkel, Viscous flow of crystalline bodies under the action of surface tension, J. Phys. (Moscow) 9 (1945) 385–391.

[30] G.C. Kuczynski, Self-diffusion in sintering of metallic particles, Trans. AIME 185 (1949) 169–178.

[31] M.S. Abd-Elhady, C.C.M. Rindt, J.G. Wijers, A.A. van Steenhoven, Particulate fouling in waste incinerators as influenced by the critical sticking velocity and layer porosity, Energy 30 (8) (2005) 1469–1479.
[32] M.S. Abd-Elhady, Gas-side particulate fouling in biomass gasifiers, Ph.D. thesis, Eindhoven University of Technology, The Netherlands, 2005.
[33] A. Bejan, Heat Transfer, John Wiley and Sons Inc, New York, 1993.
[34] H. Müller-Steinhagen, Heat Exchanger Fouling-Mitigation and Cleaning Technologies, Publico Publications, Essen, Germany, 2000.
[35] H.U. Zettler, M. Weib, Q. Zaho, H. Müller-Steinhagen, Influence of surface properties and characteristics on fouling in plate heat exchangers, Heat Transfer Eng. 26 (2) (2005) 3–18.
[36] H.F. Fischmeister, Characterization of porous structures by stereological measurements, Powder Metall. Int. 7 (4) (1975) 178–187.
[37] E.E. Underwood, Quantitative Stereology, Addison-Wesley Publishing Company, Massachusetts, 1970.
[38] A.L. Robinson, S.G. Buckley, N. Yang, L.L. Baxter, Experimental measurements of the thermal conductivity of ash deposits: part 2. Effects of sintering and deposit microstructure, Energy Fuels 15 (2001) 75–84.
[39] P. Compo, R. Pfeffer, G.I. Tardos, Minimum sintering temperature and defluidization characteristic of fluidizable particles, Powder Technol. 51 (1987) 85–101.
[40] R.M. German, Sintering Theory and Practice, John Wiley and Sons Inc, New York, 1996.
[41] T. Heinzel, V. Siegle, H. Spliethoff, K.R.G. Hein, Investigation of slagging in pulverized fuel co-combustion of biomass and coal at a pilot-scale test facility, Fuel Process. Technol. 54 (1998) 109–125.